A Survey of Unbalanced Flow Diagnostics and Their Application①

Zhang Fuqing and Steven E. Koch

Department of Marine, Earth, and Atmospheric Sciences, North Carolina State University, Raleigh, North Carolina 27695–8208, *USA*

Christopher A. Davis

National Center for Atmospheric Research, Boulder, Colorado 80307–3000, *USA*

Michael L. Kaplan

Department of Marine, Earth, and Atmospheric Sciences, North Carolina State University, Raleigh, North Carolina 27695–8208, *USA*

(Received June 9, 1999; revised November 11, 1999)

ABSTRACT

This paper presents an extensive survey of the most commonly used tools for diagnosing unbalanced flow in the atmosphere, namely the Lagrangian Rossby number, Psi vector, divergence equation, nonlinear balance equation, generalized omega–equation, and departure from fields obtained by potential vorticity (PV) inversion. The basic theory, assumptions as well as implementation and limitations for each of the tools are all discussed.

These tools are applied to high–resolution mesoscale model data to assess the role of unbalanced dynamics in the generation of a mesoscale gravity wave event over the East Coast of the United States. Comparison of these tools in this case study shows that these various methods agree to a large extent with each other though they differ in details.

Key words: Unbalanced flow, Geostrophic adjustment, Gravity waves, Nonlinear balance equation, Potential vorticity inversion, Omega equations, Rossby number

1. Introduction

Imbalance is defined in terms of to what extent the flow departs from a balanced state. Despite the apparent complexity of atmospheric motions, the pressure (mass field) and velocity (momentum) distribution can be related by rather simple approximate force balances (so that parcel accelerations can be ignored). Davis et al. (1996) pointed out that the underlying assumption of balanced diagnostics is that the flow evolves in a way consistent with the restrictions implicit within the diagnostic framework.

The simplest two balance relations are *geostrophic* balance and *hydrostatic* balance. *Hydrostatic balance* is always satisfied in the basic state of all synoptic and most mesoscale phenomena which is of interest here in while *geostrophic balance* is quite an idealistic state which rarely is strictly satisfied in the real atmosphere. Thus, *ageostrophy* (the departure away from the geostrophic balance) nearly always exists and geostrophic adjustment (leading to the

①Corresponding author's address: Dr. Fuqing Zhang, National Center for Atmospheric Research, Boulder, Colorado, 80307–3000, USA. Email: fzhang@ucar.edu.

generation of inertial gravity waves) is a primary mechanism by which the flow is brought back to a state of balance (i.e. geostrophy) (Rossby, 1938; Cahn, 1945; Blumen, 1972; Van Tuyl and Young, 1982; Koch and Dorain, 1988). An atmosphere that obeys the quasi– or semi–geostrophic system of equations can also be spoken of as being balanced. Though parcel accelerations do exist, the mass and momentum fields remain in a higher level of balance with one another, which are respectively referred to as quasi–geostrophic balance and semi–geostrophic balance.

Various Rossby numbers (*Ro*) have been suggested to be the indication of the flow imbalance (mainly the degree of ageostrophy), and used in the study of jet streaks, frontogenesis, gravity waves, mesoscale convective systems, cyclogenesis and geostrophic adjustment (Keyser and Shapiro, 1986; Koch and Dorian, 1988; Uccellini and Koch, 1987; Uccellini and Johnson 1979; Uccellini et al., 1985, 1987). These include the nonlinear advective *Ro*, the full Lagrangian *Ro*, and the cross–stream component of the Lagrangian *Ro*.

The Psi vector was developed to study the 3–D ageostrophy of balanced jet / front systems in the presence of strong curvature (Loughe et al., 1995; Xu and Keyser, 1993; Keyser et al., 1989). The Psi vector represents a 3–D generalization of the streamfunction defined by the Sawyer–Eliassen equation which is restricted to the study of straight jet–front systems under the semi–geostrophic balance constraint (Keyser and Shapiro, 1986).

The generalized omega–equation of Krishnamurti (1968) also can be used to study the flow imbalance. According to the partitioning of each term's contribution to the vertical motion, various forcing mechanisms for the balanced vertical motion can be diagnosed. The generalized omega–equation includes factors such as tilting, diabatic heating and friction that are neglected in the simple adiabatic, frictionless, quasi–geostrophic (QG) framework in which vertical motion is induced only by the advection of temperature and vorticity (Holton, 1992). The balance condition must be physically realizable in the sense that static instability, inertial instability, and the related symmetric instabilities are all absent.

Quasi–geostrophic balance (which gives the linear balance equation) has obvious limitations on time scales of the order of, or less than, the inverse of the Coriolis parameter. It is thus not generally applicable to mesoscale dynamics where the Lagrangian Rossby number is of order unity.

The Nonlinear Balance Equation (NBE), which is applicable on shorter time scales and includes the effects of curvature, is the most widely used balance condition (Charney, 1955; Hoskins et al., 1985; Allen, 1991; Raymond, 1992). The NBE is approximately valid when circulations are nearly horizontal, and it is obtained in most cases through scale analysis of the divergence equation by dropping all terms containing the divergence, the vertical velocity, and the divergent components of horizontal velocity. Allen (1991) developed a model in which more terms are retained in the divergence equation than the NBE, at the expense of allowing high frequency modes including gravity waves, though these can be easily suppressed. Moore and Abeling (1988) directly applied the divergence equation to the analysis of special rawinsonde data. Upon calculating all the terms of the divergence equation, they discussed how the nonzero sum of the terms in the NBE indicated flow imbalance dominated by the divergence tendency. The use of the divergence equation in numerical weather prediction studies can be found in House (1961), Kaplan and Paine (1977), Van Tuyl and Young (1982), Kaplan et al. (1984), and Zack and Kaplan (1987).

Davis and Emanuel (1991) argued that the balanced flow could be retrieved from Ertel potential vorticity (EPV), provided that the balanced part of the flow is mainly nondivergent while the "unbalanced" part is due to divergence. *However, the divergence tendency may be more precisely related to the existence of flow imbalance.* Potential Vorticity (PV) inversion, which usually involves solving one or more elliptic equations, is another useful way to diagnose the "imbalance". After specifying some kind of balance condition (Hoskins et al., 1985), either starting from the known mass distribution to get the balanced momentum distribution, or vice versa, the difference between the real (observed) field and derived balanced field is the imbalance (Van Tuyl and Young, 1982; Houghton et al., 1981). Sometimes the balance condition is specified by a third variable such as potential vorticity, and several inversions of the elliptic equations are required to be solved either individually or simultaneously (Raymond, 1992; Davis and Emanuel, 1991; Allen, 1991; Raymond and Jiang, 1990; Hoskins et al., 1985). Boundary conditions are always very crucial to the solutions, and sometimes they might be too complex to be specifiable (e.g. in the presence of complex terrain or strong convection).

No single method mentioned above can be totally sufficient for the study of unbalanced flow. Each method has its advantages and disadvantages (either theoretical or numerical limitations). In this study, a survey of the above diagnostics is given in Section 2. Comparative implementation of these imbalance diagnostic tools will be presented in Section 3. A brief summary and discussion appears in the last section.

2. Unbalanced flow diagnostic tools

2.1 *Rossby number*

The Lagrangian Rossby number is defined as the ratio of parcel acceleration to Coriolis acceleration:

$$Ro = \frac{|dV/dt|}{f|V|}, \tag{1}$$

while the frictionless equation of motion is

$$\frac{dV}{dt} = fV_{ag} \times k. \tag{2}$$

From (1) and (2) it is easy to redefine the Lagrangian Rossby number for frictionless flow as Koch and Dorian (1988):

$$Ro = \frac{|dV/dt|}{f|V|} = \frac{|fV_{ag} \times k|}{f|V|} = \frac{|V_{ag}|}{|V|}. \tag{3}$$

In fact, Ro as defined in (3) is simply a measure of ageostrophy, which is the departure from geostrophic balance. It can be demonstrated that in the semi-geostrophic system $Ro \ll 1$ (Hoskins, 1975). This Lagrangian Rossby number criterion for balance flow in the quasi and semi-geostrophic system is much less restrictive than the Eulerian Rossby criterion for quasi-geostrophic balance obtained from scaling considerations (Emanuel, 1986):

$$Ro = V/fL \ll 1. \tag{4}$$

The conventional definition of Ro is difficult to compute with equation (1) using observational data because of the local wind tendency term. Several approximate approaches

have been used. Uccellini et al. (1984) assessed the contribution of the inertial–advective term to the breakdown of the GM approximation in their case by calculating the " advective" Rossby number:

$$Ro \sim \frac{|V \cdot \nabla V|}{f|V|} \tag{5}$$

which ignores the local wind tendency. They found values of $Ro > 0.9$ in the exit region of the geostrophic wind maximum, further indicating that the flow was unbalanced in the same region where the ageostrophic motions were directed toward the cyclonic side of the jet. A more exact method of estimating the Lagrangian Rossby number useful as an independent measure of the degree of imbalance is (Koch and Dorian, 1988):

$$Ro \approx \frac{|V_{ag}{}^{\perp}|}{|V|} \tag{6}$$

This is quite similar to (3) except that they used the ratio of the ageostrophic wind normal to the flow to the total ageostrophic wind because they assumed that the alongstream ageostrophic wind should be governed by gradient wind balance. Accordingly, they proposed that the cross–stream ageostrophic flow directed toward the cyclonic side of the jet should be used to assess unbalanced flow in the exit region of the geostrophic jet.

2.2 *Psi vector*

Keyser et al. (1989) developed a methodology to adopt a generalized two–dimensional streamfunction, *Psi vector*, which can be uniquely determined under certain boundary conditions and describes the vertical velocity and the horizontal irrotational flow. A key property of the Psi vector is that its projections onto arbitrary orthogonal vertical planes yield two independent vertical circulations, providing an objective means for separating a three–dimensional vertical circulation into cross– and alongfront components. The Psi vector is defined as:

$$V_{agir} = -\frac{\partial \psi}{\partial p}, \quad \omega = \nabla_p \cdot \psi \tag{7}$$

where $\mathbf{V}_{agir}$ is the irrotational part of the ageostrophic wind and ω is the vertical velocity in pressure coordinates. Note that the ageostrophic wind also contains a nondivergent component, which can display both alongstream and cross–stream subcomponents. Mass continuity is guaranteed in each of the two arbitrarily defined orthogonal planes.

Loughe et al. (1995) modified the methodology for determining the Psi vector to be suitable for real limited area data–simulations with the following procedure. First, one calculates the geostrophic wind from geopotential height:

$$f_0 V_g = k \times m \nabla_p \varphi \tag{8}$$

where m is the map–scale factor. Next, which is the most important step, the ageostrophic wind is partitioned into harmonic, rotational, and divergent parts:

$$V_{ag} = V_{agh} + V_{agr} + V_{agir} \tag{9}$$

using the version of the staggered grid described by Lynch (1988) applicable to the case where the tangential wind component is specified on the lateral boundaries.

Following the partition of ageostrophic wind, the kinematic vertical motion ω is deter-

mined with the well-known approach of O'Brien (1970). Neglecting the influence of terrain and assuming ω vanishes at the lower boundary (1000 hPa), then integrate the continuity equation upward, applying a linear correction to horizontal divergence to ensure that ω vanishes at the upper boundary (100 hPa). Given the three-dimensional distribution of ω, the velocity potential χ is inverted subject to homogeneous Dirichlet conditions on lateral boundaries from

$$\omega = -m^2 \nabla_p^2 \chi. \tag{10}$$

Streamfunction ψ is diagnosed from:

$$\psi = -m \nabla_p \chi \tag{11}$$

and the divergent ageostrophic wind is determined from:

$$V_{\text{agd}} = m \nabla_p \frac{\partial \chi}{\partial p}. \tag{12}$$

The Psi vector components are then used to determine the projections of the divergent ageostrophic circulation onto orthogonal vertical planes, to be referred as the cross- and alongfront planes. A right-handed Cartesian coordinate system (s,n) oriented such that s and n denote the cross- and alongfront directions is used to define the plane. The resulting projection is:

$$v_{\text{agds}} = -\frac{\partial \psi_s}{\partial p}, \quad v_{\text{agdn}} = -\frac{\partial \psi_n}{\partial p}, \tag{13}$$

$$\omega_s = m^2 \frac{\partial}{\partial s}\left(\frac{\psi_s}{m}\right), \quad \omega_n = m^2 \frac{\partial}{\partial n}\left(\frac{\psi_n}{m}\right), \tag{14}$$

where the alongfront (s,p) plane circulation is defined by the $(v_{\text{agds}}, \omega_s)$ components and the cross-front (n,p) plane is given by circulation $(v_{\text{agdn}}, \omega_n)$. Projecting ψ onto the cross- and along front planes is achieved computationally by rotating the x and y components of ψ into the s and n directions. Vertical motion partitioning is calculated accordingly. The kinematically derived ω field also is used to provide lateral boundary conditions when solving the QG omega equation.

Application of the above methodology to two cases studies using real data over a limited area by Loughe et al. (1995) showed that the cross-stream component of the divergent ageostrophic circulation isolates meaningful mesoscale signatures coinciding with regions of precipitation and ascent in the vicinity of upper level jet-front systems, whereas the alongstream component is indicative of synoptic scale (baroclinic wave scale) vertical motion. Furthermore, they also found that the cross-contour ageostrophic flow, necessary for Lagrangian rates of change of kinetic energy in jet entrance and exit regions, is due primarily to the nondivergent (i.e., harmonic plus rotational)ageostrophic winds. This result suggests that the practice of linking cross-contour ageostrophic winds and vertical motions in jet entrance and exit regions in the quantitative assessment of energy transformations in these regions may be problematic in the case of upper-level jet-front systems situated in three-dimensional flows (Loughe et al., 1995). However, the whole Psi vector technique is built solely upon the vertical motion (which may not be accurately estimated or predicted), and the basic assumption of mass continuity will break down in the presence of high terrain.

2.3 *NBE and divergence equation*

The full divergence equation in pressure coordinate can be written as:

$$\underset{\text{A}}{\partial D/\partial t} = \underset{\text{A}}{-V\cdot\nabla D} \underset{\text{B}}{-\omega\partial D/\partial P} \underset{\text{C}}{-D^2} \underset{\text{D}}{-\partial V/\partial P\cdot\nabla\omega} \underset{\text{E}}{+2J(u,v)} \underset{\text{F}}{-\beta u} \underset{\text{G}}{+f\zeta} \underset{\text{H}}{-\nabla^2\Phi} \quad (15)$$

Terms A and B are the horizontal and vertical advection of divergence, respectively. Term C represents the nonlinear effects of the divergence. Term D is the contribution to the divergence tendency due to the vertical wind shear interaction with the gradients of vertical motion. The Jacobian term, E, is large in regions where the horizontal wind shear is strong as in the vicinity of jet streaks. The Beta term, F, can be shown by a scale analysis to be smaller than the other terms especially at the mesoscale. Term G, the relative vorticity term, can be combined with the Laplacian of the geopotential height, term H, resulting in the ageostrophic vorticity, $f\zeta'$ (House, 1961). When terms E–H sum to zero, a balanced condition is said to exist between the mass and momentum distributions as defined by the nonlinear balance equation. Significant nonzero summation of the terms E–H has been used by Moore and Abeling (1988), Zack and Kaplan (1987), Uccellini et al. (1984), and Kaplan and Paine (1977) to indicate the "breakdown" of the mass and momentum balance in the area of jet streaks or convection (subsynoptic or mesoscale phenomena). If mesoscale is defined as the lack of "large-scale" balance as by Doswell (1987), the lack of large scale balance and the response of the atmosphere to the imbalance can be well described through the divergence and vertical motion terms A–D which represent mesoscale processes.

From the diagnostic analysis of the divergence equation using rawinsonde data at upper-levels during AVE-SESAME I, Moore and Abeling (1988) conclude that the dominant contributor to the imbalance was ageostrophic vorticity. The flow was neither in geostrophic balance nor merely responding to curved flow described by the gradient wind equation. Divergence production ($\partial D/\partial t$) and mid-level upward vertical motion simultaneously increased the imbalance while the remaining part of the divergence equation (terms A–D) which includes the divergence effect itself and vertical motion, partially compensated for the strong divergence tendencies created from terms E–H. They also gave the responses of the balanced flow. The terms in the divergence equation can be more easily and accurately computed with numerical model fields than from observations.

If terms A–D in the divergence equation above and the divergence tendency are negligible, we get the general nonlinear equation (NBE):

$$\underset{\text{E}}{2J(u,v)} \underset{\text{F}}{-\beta u} \underset{\text{G}}{+f\zeta} \underset{\text{H}}{-\nabla^2\Phi} = 0. \quad (16)$$

A similar form of the nonlinear balance equation was first derived by Charney (1955) for separating the wind field into a nondivergent and an irrotational part. Following Haltiner and Williams (1980), by defining two Rossby numbers:

$$R_\psi = V_\psi / f_0 L, \text{ and } R_\chi = V_\chi / f_0 L, \quad (17)$$

retaining $O(R_\psi)$ terms but neglecting terms $O(R_\chi)$ and higher in accordance with our balance assumption, the nonlinear balance equation may also be expressed as:

$$\nabla^2\Phi = \nabla\cdot(f\nabla\Psi) + 2J(\partial\Psi/\partial x, \partial\Psi/\partial y) \quad (18)$$

with Φ the geopotential, χ the velocity potential ($\mathbf{V}_\chi = -\nabla\chi$), and Ψ the nondivergent streamfunction ($\mathbf{V}_\psi = k\times\nabla\Psi$). This equation will reduce to geostrophic balance if f is constant and the Jacobian term is neglected.

NBE states a unique relationship between the balanced mass (geopotential) and momentum (geostrophic streamfunction) fields, and has been widely used in the diagnostics of the unbalanced flow. Houghton et al. (1981) used the NBE to isolate and describe gravity–inertial waves (motions) in the output of a nonlinear (primitive equation) model of a two–layer atmosphere. They presupposed that atmospheric motions could be decomposed into two components: (1) the quasi–geostrophic or balanced state describing the general evolution of large–scale features, and (2) the unbalanced gravity–inertial component incorporating both adjustment processes of the large scale and structures with smaller scale energy sources. The quasi–geostrophic omega equation and NBE (Krishnamurti, 1968) were used diagnostically to define filtered reference data with the difference between those solutions and those from the primitive equation systems being interpreted as the gravity–inertial component. To arrive at the balanced pressure field, the primitive equation streamfunction and the balanced streamfunction were set equal enabling calculation of the geopotential via NBE. To arrive at the balanced velocity field, the primitive equation geopotential and balanced geopotential were set equal enabling calculation of the streamfunction via the balance equation.

NBE is very accurate in flows with large curvature because it is quite similar to the gradient wind balance (Davis and Emanuel, 1991). However, NBE sometimes could be hyperbolic over part of the area of interest. Krishnamurti (1968) suggested a substitute for the NBE as:

$$\nabla \cdot (f\nabla\Psi) = \nabla^2\Phi - 2J(u_g, v_g). \tag{19}$$

Comparison of the two forms (18 vs. 19) for an example with no hyperbolic regions showed very slight differences. The ellipticity condition is frequently expressed by the relation:

$$\nabla^2\Phi - \nabla \cdot (f\nabla\Psi) + 1/2f^2 > 0 \tag{20}$$

or simply evaluated as:

$$\nabla^2\Psi > -f/2. \tag{21}$$

The relation is generally satisfied by the solution over most regions except where the magnitude of the anti–cyclonic vorticity is large (inertially unstable regions).

Krishnamurti (1968) also discussed the boundary condition at the meridional limits $y = y_1$ and $y = y_2$ for the balanced model, where $\Psi = \Phi/f$ is assumed at y_1 and y_2 if the balanced equation is solved for observed geopotential distribution. The streamfunction in the boundary region is then modified to assure no net outflow through the boundary.

2.4 *Omega equations*

The traditional adiabatic and frictionless QG w–equation is

$$\nabla^2\sigma\omega + f^2\frac{\partial^2\omega}{\partial p^2} = f_0\frac{\partial}{\partial p}\left(V_g \cdot \nabla\zeta_a\right) - \nabla^2\left(V_g \cdot \nabla\frac{\partial\varphi}{\partial p}\right) \tag{22}$$

where the two forcing terms here are vertically differentiable geostrophic vorticity advection and Laplacian of geostrophic thermal advection. By separating the "balanced" vertical motion in the Q–G framework from the total vertical motion in the numerical model, the unbalanced (non–QG) vertical motion can be found which indicates the flow imbalance caused by factors other than those on the right hand side of (22).

The generalized vertical motion equation used by Krishnamurti (1968) is

$$\nabla^2\sigma\omega + f^2\frac{\partial^2\omega}{\partial p^2} = f\frac{\partial}{\partial p}J(\psi,\zeta_a) + \pi\nabla^2 J(\psi,\theta) - 2\frac{\partial}{\partial t}\frac{\partial}{\partial p}J(\frac{\partial\psi}{\partial x},\frac{\partial\psi}{\partial y}) - f\frac{\partial}{\partial p}(\zeta\nabla^2\chi)$$

$$L(\omega) \qquad A \qquad B \qquad C \qquad D$$

$$+ f\frac{\partial}{\partial p}g\frac{\partial}{\partial p}\left[\frac{\partial\tau_y}{\partial x} - \frac{\partial\tau_x}{\partial y}\right] - \frac{R}{c_p P}\nabla^2 H_L - \frac{R}{c_p P}\nabla^2 H_S + f\frac{\partial}{\partial p}(\omega\frac{\partial}{\partial p}\nabla^2\psi) \qquad (23)$$

$$E \qquad F \qquad G \qquad H$$

$$f\frac{\partial}{\partial p}\left(\nabla\omega\cdot\nabla\frac{\partial\psi}{\partial p}\right) - f\frac{\partial}{\partial p}(\nabla\chi\cdot\nabla\zeta_a) - \pi\nabla^2(\nabla\chi\cdot\nabla\theta) - \beta\frac{\partial}{\partial p}\frac{\partial}{\partial y}\frac{\partial\psi}{\partial t}.$$

$$I \qquad J \qquad K \qquad M$$

The 12 forcing functions on the right hand side of the equation are: A, Differential vorticity advection by the nondivergent part of the wind; B, Laplacian of the thermal advection by the nondivergent part of the wind; C, Differential deformation effect (shear term); D, Differential divergence effects of a balance model; E, vertical Laplacian of frictional stresses; F, Laplacian of the latent heating; G, Laplacian of sensible heat transfer from the surface to the atmosphere; H, Differential vertical advection of vorticity; I, Differential turning of vortex tubes (tilting effect); J, Differential advection of vorticity by the divergent part of the wind; K, Laplacian of thermal advection by the divergent part of the wind; M, Contribution by the beta term of the divergence equation.

Generally, if a forcing function term is greater than zero, then in the vicinity of this region its contribution will be rising motion. But noticeably, the terms of the QG omega–equation do not exactly correspond to the first two terms in (23) because the streamfunction used in QG theory is the geostrophic frictionless $\Psi = \Phi / f$ while for the latter case the balanced nondivergent streamfunction is used (see details in NBE section). In addition, f is constant and static stability is a function of pressure only in the QG system, while in the generalized omega–equation their horizontal variation contributes. The heating terms F and G will in general contribute rising motions since $\nabla^2 < 0$ where maxima exist. Frictional stress term E will generally contribute rising motion in regions of cyclonic relative vorticity and sinking motion in the regions of anticyclonic relative vorticity. The deformation and the divergence term C and D may be very large near frontal systems and other mesoscale phenomena (though their interpretation is somewhat difficult). Term M is comparatively much smaller than any of the other terms.

A partitioning of each forcing term's contribution to the vertical motion is possible and then individual effects of each term on the flow can be determined uniquely just like what is done in QG theory. But such a partitioning cannot in general be done using inhomogeneous boundary conditions (like terrain contributions) because they will enter into all terms so that $\omega = \sum\omega_i$ will not hold. The forcing functions by themselves are very cellular while the ω–field is better defined. This is analogous to the relation between vorticity and streamfunction.

The NBE which is used to solve the ω–equation can become hyperbolic over portions of the region for various reasons like heating functions or terms D and I when smaller mesh size of order or less than 100 km is considered. These problems will be discussed in detail in the methods to be used for obtaining a solution of NBE.

The generalized omega–equation in sigma–coordinate can be achieved with similar derivation and assumptions used by Krishnamurti (1968).

$$\nabla^2 S\dot{\sigma}+f^2\frac{\partial^2\dot{\sigma}}{\partial\sigma^2}=-f\frac{\partial}{\partial\sigma}J(\psi,\zeta_a)-\nabla^2[\frac{\pi R}{p}J(\psi,T)]-2\frac{\partial^2}{\partial t\partial\sigma}(J(\frac{\partial\psi}{\partial x},\frac{\partial\psi}{\partial y})$$
$$+f\frac{\partial}{\partial\sigma}(\zeta\nabla^2\chi)-\frac{\partial}{\partial\sigma}\{f\vec{k}\cdot[\nabla\times\vec{F}]\}+\nabla^2(\frac{\pi R}{p}Q)-f\frac{\partial}{\partial\sigma}(\dot{\sigma}\frac{\partial\nabla^2\psi}{\partial\sigma})$$
$$-f\frac{\partial}{\partial\sigma}(\nabla\dot{\sigma}\cdot\nabla\frac{\partial\chi}{\partial\psi})+f\frac{\partial}{\partial\sigma}(\nabla\chi\cdot\nabla\zeta_a)+\nabla^2(\frac{\pi R}{p}\nabla\chi\cdot\nabla T)$$
$$-\frac{\partial}{\partial\sigma}\{f\vec{k}\cdot[\nabla(\alpha\sigma)\times\nabla\pi]\}-\frac{\partial^2}{\partial t\partial\sigma}[\nabla\cdot(\alpha\sigma\nabla\pi)]-f^2\frac{\partial^2}{\partial\sigma^2}\frac{\dot{\pi}}{\pi},\qquad(24)$$

where the stability parameter $S=\dfrac{\pi R}{p}\dfrac{\partial T}{\partial\sigma}$.

The left hand side of (24) and the firsst 10 terms on the right hand side are quite similar in form and have similar physical meaning to those in (23) by Krishnamurti (1968). Linear low-level boundary conditions are automatically satisfied in the terrain following coordinates while the last three terms are added due to the terrain effects.

2.2.5 *PV inversion*

The quasi-geostrophic pseudo-potential vorticity (PPV, Charney and Stern, 1962) which is a commonly used approximation of Ertel PV is defined:

$$q_b=\nabla^2\psi+f_0+\beta(y-y_0)+\frac{f_0^2}{\bar{\rho}}(\frac{\bar{\rho}}{N^2}\psi_z)_z\qquad(25)$$

while in a fully baroclinic, compressible flow the generalized Ertel's potential vorticity (EPV, Rossby, 1938; Ertel, 1942) is:

$$q=\frac{1}{\rho}\eta\cdot\nabla\theta.\qquad(26)$$

Thorpe and Emanuel (1985) and Haynes and McIntyre (1987) remarked that potential vorticity (in a mass integrated sense) cannot be created or destroyed, except at the earth's surface.

Davis and Emanuel (1991) assumed that the irrotational part of the horizontal wind is relatively small. Under this condition, there is a unique linear (elliptic) relationship between the geopotential height Φ and the balanced streamfunction Ψ through nonlinear balance equation:

$$\nabla^2\Phi=\nabla\cdot(f\nabla\Psi)+2m^2J_{xy}(\partial\Psi/\partial x,\partial\Psi/\partial y).\qquad(27)$$

According to the definition of EPV and scaling approximation, potential vorticity has the following relation with geopotential height and balanced streamfunction:

$$q=\frac{q\kappa\pi}{p}\left[(f+m^2\nabla^2\Psi)\frac{\partial^2\Phi}{\partial\pi^2}-m^2\frac{\partial^2\Psi}{\partial x\partial\pi}\frac{\partial^2\Phi}{\partial x\partial\pi}-m^2\frac{\partial^2\Psi}{\partial y\partial\pi}\frac{\partial^2\Phi}{\partial y\partial\pi}\right].\qquad(28)$$

So given the three-dimensional potential vorticity field q from a model, under certain boundary conditions, two elliptic equations (27) and (28) form a complete system and can be solved numerically for the two unknown variables: balanced Φ and Ψ.

For boundary conditions Φ and Ψ on the lateral boundaries are prescribed and their vertical derivatives are specified. The modeled (observed) geopotential serves as Φ on the lateral

edges and the hydrostatic equation

$$\frac{\partial \varphi}{\partial \pi} = -\theta \tag{29}$$

is applied at the top and bottom. The gradient of Ψ along the edge should match the normal wind component

$$\frac{\partial \Psi}{\partial s} = -v \cdot n + \frac{\oint v \cdot n dl}{\oint dl} \tag{30}$$

where n is the outward normal and s is parallel to the edge (counterclockwise). The last term in (30) subtracts net divergence in the domain and forces the integral of $\frac{\partial \Psi}{\partial s}$ around the edge to vanish. The arbitrary constant of integration is supplied by specifying $\Phi = \Psi$ at one point on the boundary. The condition for Ψ on the horizontal boundaries is

$$\frac{\partial \Psi}{\partial \pi} = -\theta \tag{31}$$

applied at the bottom and the top. This is justified because the term involving the vertical dirivative of Ψ in (31) is already $O(R_\Psi)$. The final solution turns out to be very insensitive to this choice of boundary condition. Davis and Emanuel (1991) use the SOR (successive overrelaxation) method to solve the elliptic equations (Robinson 1988 also use SOR method). As long as the EPV is positive everywhere, in the 3D domain, a convergent solution is obtainable. Their tests with different initial guesses showed that the solution obtained was apparently unique (which is questionable in strict mathematics sense because of the nonlinearity of the equations), or at least other existing solutions were unreachable. In this case study, they showed that the "balanced flow" obtained by the above method accurately reflects the observed winds, with nearly all the differences attributable to divergence. (This is surely because the use of the NBE). They further developed the method applied to piecewise EPV inversion and suggested that it is perhaps the most useful diagnostic application of the invertibility principle. When the invertibility relation is linear, piecewise inversion is a Green's function technique, for one can imagine inverting an array of the point source PV anomalies whose circulation sums to the total flow. Negative PV values are set to a small positive constant.

3. Application of the imbalance diagnostics to gravity wave generation

A large–amplitude gravity wave event was recently documented by Bosart et al. (1998), hereafter B98, with conventional surface and upper–air observations. The average phase speed of the wave as it propagated from Virginia to Massachusetts was 27 m s $^{-1}$. Its wavelength was 100 km with a peak crest–to–trough pressure fall of 13 hPa in 20–30 minutes. The gravity wave was one of the three prominent mesoscale features associated with the cyclone, the others being a weak offshore warm–frontal wave that reinforced the wave duct preceding the gravity wave and a heavy snow band ("snow bomb") along the Appalachians. Unbalanced flow and associated geostrophic adjustment was hypothesized to be one of the most likely mechanisms for generating the gravity wave. However, as they stated, lack of critical observations and limited data resolution prevented them from determining the actual organizing dynamics of the gravity waves as well as the role of diabatic heating and terrain effects. In this section, most of the advanced unbalanced flow diagnostics discussed in the previous

section are applied to high-resolution numerical simulations to assess the role of unbalanced dynamics in gravity wave generation.

The NCAR / PSU Mesoscale Model 5 (MM5) Version 2 (Grell et al., 1995) was used with horizontal grid sizes of 36 km and 12 km. The coarse domain was initialized at 0000 UTC 4 January 1994 with conventional data and the 12-km nested domain was spawned at 0300 UTC. The MM5 simulated results compare well with the synoptic-scale observational analysis and replicate the Eta model features such as 300 hPa jet core strength and location, ageostrophic winds (not shown), the surface cyclone and precipitation (Fig. 1). Moreover, the model shows strong skill in forecasting the three prominent mesocale features, i.e., dominant large-amplitude gravity wave (Fig. 2), snow band (Figs. 1 and 2) and precursor

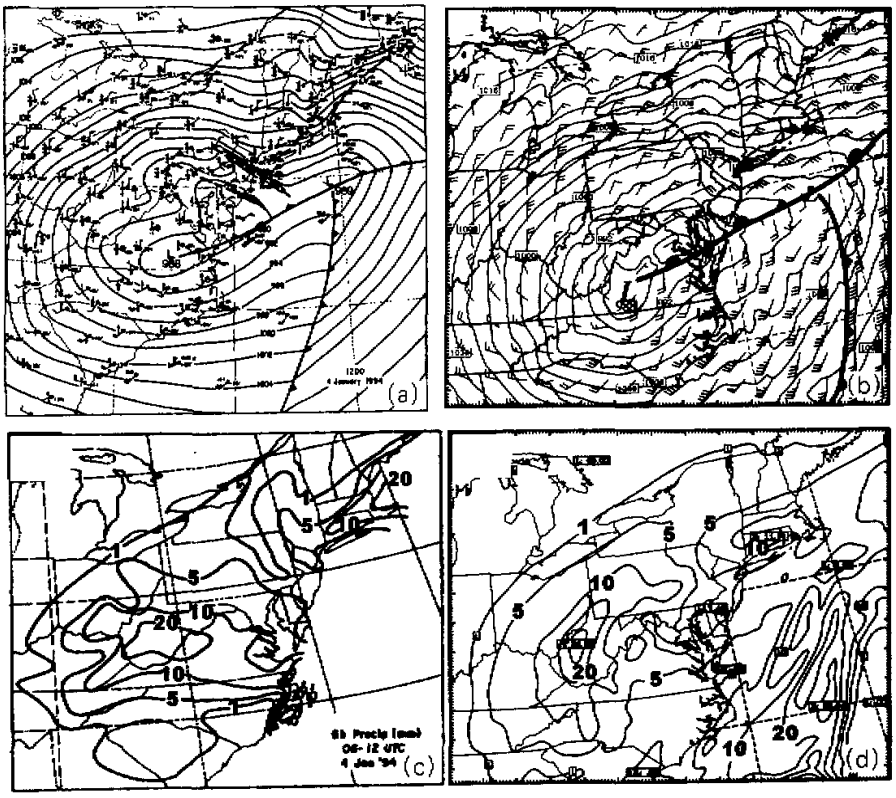

Fig. 1. (a) Observational surface analysis for 1200 UTC 4 January 1994 (Bosart, et al., 1998). Mean sea level isobars (soild, every 2 hPa). (c) Observed accumulated precipitation (solid, contoured every 1,5,10, and 20 mm) from 0600 to 1200. (b), and (d) are as in panels (a) and (c) except for the MM5 simulated fields. Dashed lines in (a) and (b) denote gravity wave trough axes.

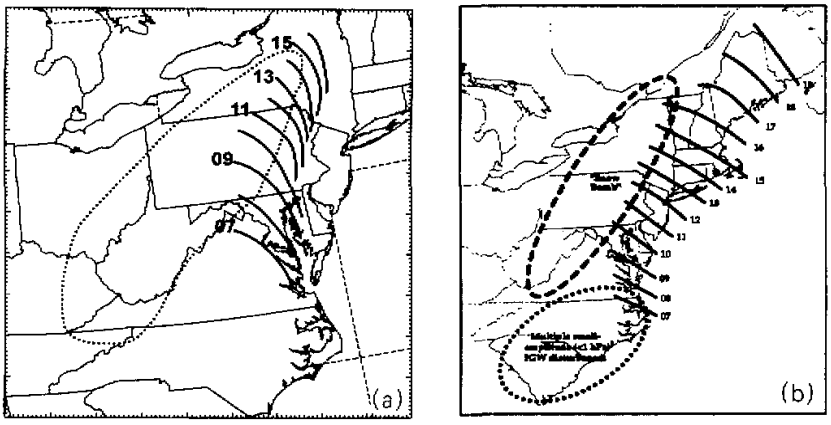

Fig. 2. (a) Isochrone analysis of simulated gravity wave for 4 January 1994. Area with accumulated precipitation from 00 to 18 UTC greater than 20 mm is outlined by dotted line. (b) Observational analysis (from Bosart et al., 1998).

warm front embedded within the cyclone. Model results show that the surface gravity wave is not related to the timing of the secondary cyclogenesis over the ocean. The MM5 simulated gravity wave was generated at 0700 UTC and propagated along the East Coast with a speed of 20 m s^{-1} before 1200 UTC. The timing and the wave speed are quite similar to those observed. Both the MM5 model and observations show that the gravity wave formed in a region near the 300 hPa inflection axis bounded by the 300–hPa ridge to the northeast, the trough axis to the southwest, and a surface warm front boundary to the southeast, which is consistent with the Uccellini and Koch (1987) conceptual model for mesoscale gravity waves.

In this study, we will apply most of the imbalance diagnostic tools reviewed in the previous section to determine whether the flow is actually unbalanced or not prior to the gravity wave generation. We will focus on the performance, similarity and difference between these tools. The evolution and the governing dynamics of the extratropical cyclone and mesoscale gravity waves of this case can be found in Zhang et al. (1999). Analysis in great detail using numerical simulations, wavelet analysis and energy transport as well as unbalanced flow diagnosis will be reported elsewhere. The Lagrangian Rossby number estimated from (3) and the residual of the Nonlinear Balance Equation (16) are shown respectively at the time when the gravity wave was just appearing in the model simulation (at 0600 UTC) in Figure 3. There is clear evidence of strong imbalance associated with a mid–upper tropospheric jet streak upstream of the gravity wave activity which is present from hour 0 (not shown) and continues even after the dissipation of the strongest gravity wave activity. Notice that the local maximum of Rossby number and NBE residual are not collocated. The maximum Rossby number ($Ro > 1.5$) is located in the deep trough region over the Gulf of Mexico where the flow is strongly subgeostrophic; the maximum NBE residue is located on the cyclonic side of the jet streak over South Carolina and Georgia border (though there is a secondary maximum of the

Rossby number ($Ro > 0.75$ over this area). The maximum NBE residual is closer to the region of gravity wave generation than that of the Rossby number. This suggests that the full Rossby number is less effective unbalance flow indicator because the maximum of the Rossby number is dominated by the curvature effect (the same is not true for formulation (6)).

Quasi-geostrophic balanced omega was also computed (Fig. 4a) and subtracted from the simulated upward motion to arrive at the non-quasigeostrophic omega fields (Fig. 4b). Figure 4 suggests that the heavy precipitation along the Appalachians ("snow bomb") is mostly forced by balanced QG dynamics while the strong convective activity off the coast is unbalanced (non-QG) forcing associated with the upper level jet streak. The balanced 300 hPa omega fields show a typical two-cell pattern associated with highly curved jet streaks. A mid-level cloud band ahead of a narrow dry conveyor belt originating from Georgia was identified as a small amplitude gravity wave by B98 (see their Fig. 12). This satellite observed cloud band correlates reasonably well with the non-quasigeostrophic omega fields and the leftward directed ageostrophic flow (Zhang et al., 1999). However, for this case studied in which the upper level jet streak is highly curved, the strongest QG upward motion over the Carolinas (indicating strong quasigeostrophic forcing shown by negative value in Fig. 4a) is generally larger than the simulated upward motion. The "unbalanced" non-quasigeostrophic vertical motion in Fig. 4b is dominated by the phase difference between the simulated vs. "balanced" upward motions more than their magnitude difference. Thus, it is not collocated with the strong imbalance shown by the NBE residual in Fig. 3b over Georgia and South Carolina. Similar to the Rossby number for highly curved flow, this imbalance diagnosis using QG omega equation is also limited by the underlying quasigeostrophic balance assumption.

The potential vorticity (PV) inversion technique originally developed by Davis and Emanuel (1991) is also applied to the MM5 model output. Fig. 5 shows balanced geopotential heights resulting from the PV inversion and the unbalanced heights at 0600Z for the coarse domain. The imbalance suggested from this analysis is very consistent with that from the NBE analysis. There is a primary maximum of unbalanced height over the South Carolina-Georgia border where the NBE residue is the largest. Also, there is a secondary maximum off the Carolina coast indicating the imbalance created by the coastal convection. This secondary imbalance maximum is also evident in the NBE residual field as well as the non-quasigeostrophic omega field. Unbalanced streamfunction field and vertical motion obtained with the same procedure display similar results to that of the unbalanced heights and will not be shown here.

The unbalanced height from PV inversion can be linked to the imbalance of NBE by the following argument because the simulated wind field (streamfunction) is nearly balanced. We have

$$\Psi \approx \Psi_B; \quad \Phi = \Phi_B + \Phi_U. \tag{32}$$

By definition,

$$2J_{xy}(\partial\Psi_B/\partial x, \partial\Psi_B/\partial y) + \nabla\cdot(f\nabla\Psi_B) - \nabla^2\Phi_B = 0, \tag{33}$$

and

$$\Delta NBE = 2J(u,v) + f\zeta - \nabla^2\Phi = 2J_{xy}(\partial\Psi/\partial x, \partial\Psi/\partial y) + \nabla\cdot(f\nabla\Psi) - \nabla^2\Phi. \tag{34}$$

So we have the relationship,

$$\Delta NBE \approx 2J_{xy}(\partial\Psi_B/\partial x, \partial\Psi_B/\partial y) + \nabla\cdot(f\nabla\Psi_B) - \nabla^2(\Phi_B + \Phi_U) - \nabla^2\Phi_U \propto \Phi_U. \tag{35}$$

The above derivation explains why the local unbalanced positive maximum of geopotential heights is often correlated to the local maximum of residual of NBE.

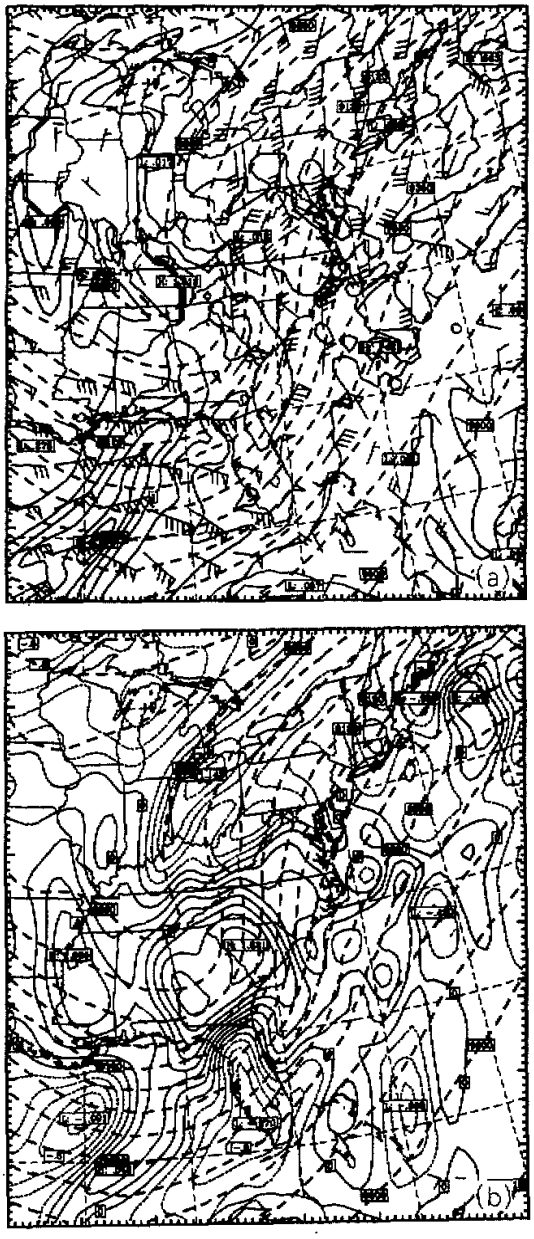

Fig. 3. (a) MM5 simulated 300-hPa geopotential heights (dashed, every 60 m) ageostrophic winds (full barb 5 m s^{-1}) and Lagrangian Rossby number (thin solid, every 0.25) (b) Simulated residual of Nonlinear Balanced Equation (thin solid, positive, dotted, negative, every $10^{-6}s^{-1}$) and geopotential heights (dashed, every 60 m) at 0600 UTC 4 January 1994.

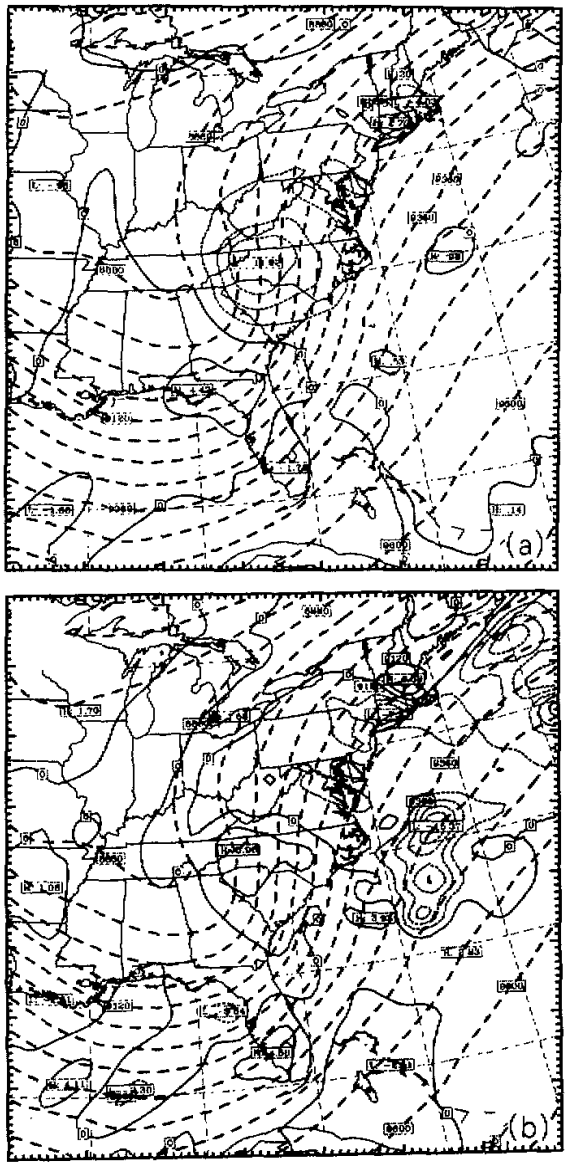

Fig. 4. Quasi-geostrophic balanced 300-hPa omega (every 3 μ pa / s^{-1}), and (b) the unbalanced 300 hPa omega obtained by subtracting balanced omega from the simulated omega at 0600 UTC 4 January 1994.

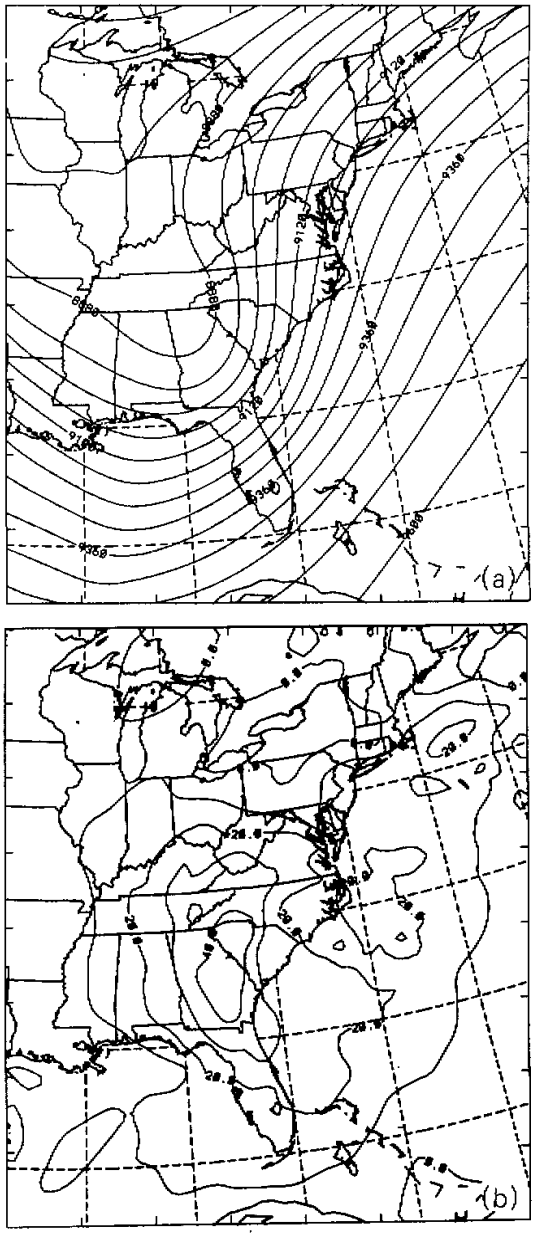

Fig. 5 (a) PV inverted balanced 300−hPa geopotential heights (every 60 m), and (b) Unbalanced 300−hPa geopotential heights (every 10 m) obtained by subtracting the balanced heights from model heights at 0600 UTC 4 January 1994.

In summary, all of these tools agree to a large extent with each other though they differ in details. Each indicator shows a local maximum of imbalance over the South Carolina / Georgia border and off the Carolina coast suggesting the upper-level flow is highly unbalanced prior to the gravity wave generation though the strongest imbalance is not collocated. The dominant gravity wave will be generated in the leading (downstream) edge of the strongest imbalance over central Virginia within the next hour through geostrophic adjustment. After the gravity wave is generated, the "localized" imbalance associated with the gravity wave grows while the orginal primary imbalance to the cyclonic side of the jet streak is decreasing. The energy associated with the strong imbalance is emanating through the release of the gravity waves. The processes how the imbalance was initiated and how the actual geostrophic adjustment process generated the observed large amplitude gravity wave are very complicated and they are presently studied and will be reported elsewhere. Of all the diagnostic tools applied in the case studied, Rossby number and the NBE residue are much easier to estimate from the model while QG-omega equation and PV inversion deserve much harder numerical efforts. The imbalance diagnosed from PV inversion and the NBE residual is considerably better and more informative than that from the Rossby number and the quasi-geostrophic omega equation because nonlinear balance is a higher-level and more realistic balance assumption for the atmosphere than geostrophy or quasi-geostrophy.

4. Summary and discussion

An extensive survey of the most commonly used unbalanced flow diagnostic tools, e.g. Rossby Number, various kinds of omega-equations, Psi vector, divergence equation, nonlinear balance equation (NBE), and PV inversion was made in this study. The basic theories, assumptions and limitations of each of the tools have been documented. Some of these tools were applied to high-resolution mesoscale model data to assess the role of unbalanced dynamics in the generation of a simulated mesoscale gravity wave event. Comparison of these tools in this case study shows that these various methods to a large extent agree with each other though they differ in details.

The Lagrangian Rossby number is a very basic imbalance indicator that is used to scale the governing equations for synoptic-scale flow (Holton, 1992). The generalized omega-equations and Psi vector are basically cast in the quasi-geostrophic framework and they are the natural three-dimensional extension of the study of ageostrophy. The Psi vector method may be used to study highly curved unbalanced jet-front systems. The NBE is the foundation of the methods of PV thinking and the generalized omega-equation. NBE is a higher level balance similar to semi-geostrophy (though it has different forms under different scale analysis). NBE and PV analyses can be easily performed upon four-dimensional mesoscale model grids. Most of the methods involve the solution of Poisson equations, in which apropriate boundary conditions are required and ellipticity of the equations must be assured, especially in the presence of steep terrain and strong diabatic heating.

There are some other methods available for diagnosing flow imbalance which have not been mentioned above. For example, the concept of nonlinear normal-mode initialization (Daley, 1980, 1991) may also be used to characterize the balanced condition, and it may be one of the best methods to separate fast inertial-gravity motion from the slow manifold mode. The basic idea is to express the fields of wind, tempeature, etc., as a superposition of modes belonging to a complete set of atmospheric linear normal modes, and then set to zero the coefficient of all modes not belonging to a subset considered representative of balanced

motion. The accuracy of the "linear balance" thus realized is then improved by iteration on the nonlinear, topographic, and forcing terms in the equations and boundary conditions. According to scale analysis shorter scale atmospheric motions tend to be more "unbalanced" than larer scale motions (Barnes et al., 1996). Based on this assumption, spectral decomposition as well as wavelet analysis can be also used to partition the flow into fast mode and slow mode parts and thus can be used as imbalance diagnostics as well. These analyses are currently being explored with the model data set presented in this paper.

This research was conducted under support from NSF grant ATM-9700626 of the United States. The numerical computations described herein were performed on the Cray T90 at the North Carolina Supercomputing Center and the Cray supercomputer at the NCAR Scientific Computing Division, which also provided the initialization fields for the MM5. Thanks are extended to Mark Stoelinga at University of Washington for the RIP post-processing package.

REFERENCES

Allen, J.S., 1991: Balance equations based on momentum equations with global invariants of potential enstrophy and energy. *J. Atmos. Sci.*, **21**, 267-276.

Barnes, S.L., F. Caracena, and A. Marroquin, 1996: Extracting synoptic scale diagnostic information from mesoscale models: The Eta model, gravity waves, and quasigeostrophic diagnostics. *Bull. Amer. Meteor. Soc.*, **77**, 519-528.

Blumen, W., 1972: Geostrophic adjustment. *Rev. Geophys. Space Phys.*, **10**, 485-528.

Bosart, L. F., W. E. Bracken, and A. Seimon, 1998: A study of cyclone mesoscale structure with emphasis on a large-amplitude inertia-gravity wave. *Mon. Wea. Rev.*, **126**, 1497-1527.

Cahn, A., 1945: An investigation of the free oscillations of a simple current system. *J. Meteor.*, **2**, 113-119.

Charney, J. G., 1955: The use of primitive equations of motion in numerical prediction. *Tellus*, **7**, 22-26.

Charney, J.G., and M.E. Stern, 1962: On the stability of internal baroclinic jets in a rotating atmosphere. *J. Atmos. Sci.*, **19**, 159-172.

Daley, R., 1980: On the optimal specification of the initial state for deterministic forecasting. *Mon. Wea. Rev.*, **108**, 1719-1735.

Daley, R., 1991: *Atmospheric Data Analysis*. Cambridge University Press. 457 pp.

Davis, C.A., and K.A. Emanuel, 1991: Potential vorticity diagnosis of cyclogenesis. *Mon. Wea. Rev.*, **119**, 1929-1952.

Davis, C.A., E.D. Grell, and M.A. Shapiro, 1996: The balanced dynamical nature of a rapidly intensifying oceanic cyclone. *Mon. Wea. Rev.*, **124**, 3-26.

Emanuel, K.A., 1986: Overview and definition of mesoscale meteorology. *Mesoscale Meteorology and Forecasting*, edited by P.S. Ray., American Meteorological Society. 1-17.

Grell G.A., J. Dudhia, and D.S. Stauffer, 1995: A description of the fifth-generation Penn State / NCAR mesoscale model (MM5). NCAR Technical Note, NCAR/ TN-398+STR, 122 pp.

Haltiner, G.J., and R.T. Williams, 1980: *Numerical Prediction and Dynamic Meteorology*, Wiley, New York.

Haynes, P.H. and McIntyre, M.E., 1987: On the evolution of vorticity and potential vorticity in the presence of diabatic heating and frictional or other forces. *J. Atmos. Sci.*, **44**, 828-841.

Holton, J.R., 1992: *An Introduction to Dynamic Meteorology*. Academic Press, 507 pp.

Hoskins, B.J., 1975: The geostrophic momentum approximation and the semi-geostrophic equations. *J. Atmos. Sci.*, **32**, 232-242.

Hoskins, B.J., M.E. McIntyre, and A.W. Robertson, 1985: On the use and significance of isentropic potential vorticity maps. *Quart. J. Roy. Meteor. Soc.*, **111**, 877-946.

Houghton, D.D., W.H. Campbell, and N.D. Reynolds, 1981: Isolation of the gravity-inertial motion component in a nonlinear atmospheric model. *Mon. Wea. Rev.*, **109**, 2118-2130.

House, D.C., 1961: The divergence equation as related to severe thunderstorm forecasting. *Bull. Amer. Meteor. Soc.*, **42**, 803-816.

Kaplan, M.L., and D.A. Paine, 1977: The observed divergence of the horizontal velocity field and pressure gradient force at the mesoscale. *Beitr. Phys. Atmos.*, **50**, 321–330.

Kaplan, M.L., J.W. Zack, V.C. Wong, and J.J. Tuccillo, 1984: The interactive role of subsynoptic scale jet streak and planetary boundary layer adjustments in organizing an isolated convective complex. *Mon. Wea. Rev.*, **113**, 2212–2238.

Keyser, D., B.D. Schmidt, and D.G. Duffy, 1989: A technique for representing three-dimensional vertical circulations in baroclinic disturbances. *Mon. Wea. Rev.*, **117**, 2463–2494.

Keyser, D., and M.A. Shapiro, 1986: A review of the structure and dynamics of upper-level frontal zones. *Mon. Wea. Rev.*, **114**, 452–499.

Klemp, J. B., and D.K. Lilly, 1978: Numerical simulation of hydrostatic mountain waves. *J. Atmos. Sci.*, **35**, 78–107.

Koch, S.E., and P. B. Dorian, 1988: A mesoscale gravity wave event observed during CCOPE. Part III: Wave environment and probable source mechanisms. *Mon. Wea. Rev.*, **116**, 2570–2592.

Krishnamurti, T.N., 1968: Diagnostic balance model for studies of weather systems of low and high latitudes, Rossby Number less than 1. *Mon. Wea. Rev.*, **96**, 197–207.

Loughe, A.F., C.-C. Lai, and D. Keyser, 1995: A technique for diagnosing three-dimensional ageostrophic circulations in baroclinic disturbances on limited-area domains. *Mon. Wea. Rev.*, **123**, 1276–1503.

Lynch, P., 1988: Deducing the wind from vorticity and divergence. *Mon. Wea. Rev.*, **116**, 86–93.

Moore, J.T., and W.A. Abeling, 1988: A diagnosis of unbalanced flow in upper levels during the AVE-SESAME I period. *Mon. Wea. Rev.*, **116**, 2425–2436.

O'Brien, J, 1970: Alternative solutions to the classical vertical velocity problem. *J. Appl. Meteor.* **9**, 197–203.

Raymond, D.J., 1992: Nonlinear balance and potential vorticity thinking at large Rossby number. *Quart. J. Roy. Meteor. Soc.*, **118**, 987–1105.

Raymond, D.J., and H. Jiang, 1990: A theory for long-lived mesoscale convective systems. *J. Atmos. Sci.*, **47**, 3067–3077.

Rossby, C.G., 1938: On the mutual adjustment of pressure and velocity distributions in certain simple current systems. II. *J. Marine Res.*, **7**, 239–263.

Thorpe, A.J., and Emanuel, K.A., 1985: Frontogenesis in the presence of small stability to slantwise convection. *J. Atmos. Sci.*, **42**, 1809–1824.

Uccellini, L.W., D. Keyser, K.F. Brill, and C.H. Wash, 1985: The Presidents' Day cyclone of 18–19 February 1979: Influence of upstream trough amplification and associated tropopause folding on rapid cyclogenesis. *Mon. Wea. Rev.*, **113**, 962–988.

Uccellini, L.W., P.J. Kocin, R.A. Petersen, C.H. Wash, and K.F. Brill, 1984: The Presidents' Day cyclone of 18–19 February 1979: Synoptic overview and analysis of the subtropical jet streak influencing the precyclogenesis period. *Mon. Wea. Rev.*, **112**, 31–55.

Uccellini, L.W., R.A. Petersen, K.F. Brill, P.J. Kocin, and J.J. Tuccillo, 1987: Synergistic interactions between an upper-level jet streak and diabatic processes that influence the development of a low-level jet and a secondary coastal cyclone. *Mon. Wea. Rev.*, **115**, 2227–2261.

Uccellini, and S.E. Koch, 1987: The synoptic setting and possible source mechanisms for mesoscale gravity wave events. *Mon. Wea. Rev.*, **115**, 721–729.

Xu, Q., and D. Keyser, 1993: Barotropic and baroclinic ageostrophic winds and completeness of solution for the Psi equations. *J. Atmos. Sci.*, **50**, 588–596.

Van Tuyl, A.H., and J.A. Young, 1982: Numerical simulation of nonlinear jet streak adjustment. *Mon. Wea. Rev.*, **110**, 2038–2054.

Zack, J. W., and M.L. Kaplan, 1987: Numerical simulations of the subsynoptic features associated with the AVE-SESAME I case. Part I: The pre-convective environment. *Mon. Wea. Rev.*, **115**, 2367–2394.

Zhang, F., S. E. Koch, M.L. Kaplan, and C.A. Davis, 1999: Numerical simulation of the role of unbalanced dynamics in the generation of a large amplitude mesoscale gravity wave. Preprints *8th Conference on Mesoscale Processes*, Boulder, Colorado, American Meteorological Society, 79–85.